HHS Public Access

Author manuscript

Bioconjug Chem. Author manuscript; available in PMC 2017 June 19.

Published in final edited form as:

Bioconjug Chem. 2017 April 19; 28(4): 1093–1101. doi:10.1021/acs.bioconjchem.7b00012.

Pre-Assembled Fluorescent Multivalent Probes for Imaging of Anionic Membranes

Felicia M. Roland, **Evan M. Peck**, **Douglas R. Rice**, and **Bradley D. Smith***

Department of Chemistry and Biochemistry, 236 Nieuwland Science Hall, University of Notre Dame, Notre Dame, Indiana 46556, USA

Abstract

A new self-assembly process known as Synthavidin (Synthetic Avidin) technology was used to prepare targeted probes for near-infrared fluorescence imaging of anionic membranes and cell surfaces, a hallmark of many different types of disease. The probes were pre-assembled by threading a tetralactam macrocycle with six appended zinc-dipicolylamine (ZnDPA) targeting units onto a linear scaffold with one or two squaraine docking stations to produce hexavalent or dodecavalent fluorescent probes. A series of liposome titration experiments showed that multivalency promoted stronger membrane binding by the dodecavalent probe. In addition, the dodecavalent probe exhibited turn-on fluorescence due to probe unfolding during fluorescence microscopy at the membrane surface. But the dodecavalent probe also had a higher tendency to self-aggregate after membrane binding leading to probe self-quenching under certain conditions. This self-quenching effect was apparent during fluorescence microscopy experiments that recorded low fluorescence intensity from anionic dead and dying mammalian cells that were saturated with the dodecavalent probe. Conversely, probe self-quenching was not a factor with anionic microbial surfaces where there was intense fluorescence staining by the dodecavalent probe. A successful set of rat tumor imaging experiments confirmed that the pre-assembled probes have sufficient mechanical stability for effective in vivo imaging. The results demonstrate the feasibility of this general class of pre-assembled fluorescent probes for multivalent targeting, but fluorescence imaging performance depends on the specific physical attributes of the biomarker target such as the spatial distance between different copies of the biomarker and the propensity of the probe/biomarker complex to self-aggregate.

TOC image

* smith.115@nd.edu.

Supporting Information

The Supporting Information is available free of charge on the ACS Publications website at DOI: 10.1021/? Synthetic procedures, compound characterization and spectral data, experimental methods, and additional imaging data.

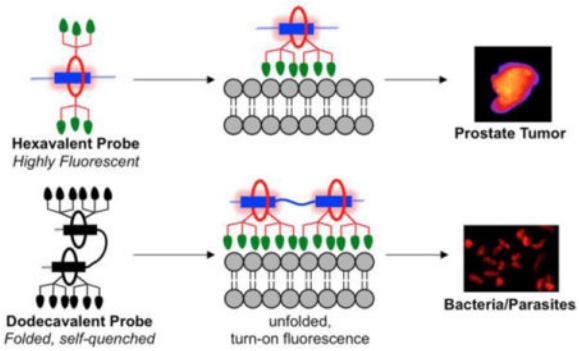

INTRODUCTION

There is a considerable ongoing effort to develop fluorescent probes that selectively target biomarkers on cell surfaces for a wide range of biological imaging techniques including cell microscopy, flow cytometry, microarray diagnostics, intravital microscopy, and in vivo imaging.[1,2] It is especially challenging to design targeted probes with the correct mixture of chemical, photophysical and pharmacokinetic properties for high performance imaging of living subjects.[3] Probe synthesis has been greatly facilitated in recent years by the development of facile covalent bond formation methods, such as high yielding click reactions, that connect the appropriate targeting and reporter building blocks.[4] However, covalent fabrication methods are often less useful for the construction of multivalent probe structures due to slower rates of reaction at the congested conjugation sites.[5,6] This means the chemical reactions must be run at high reaction temperatures and use reagents in stoichiometric excess, which in turn may require tedious product purification steps. In principle, multivalent probe fabrication can also be achieved using methods based on non-covalent self-assembly; however, this idea remains underdeveloped due to the scarcity of robust, high-affinity self-assembly systems.[7,8] In an effort to address this deficiency, we are developing a programmable self-assembly synthesis method that can produce libraries of targeted near-infrared fluorescent probes with multiple targeting ligands.[9,10] We refer to the basic self-assembly process as Synthavidin (Synthetic Avidin) technology.[11] To briefly summarize, a tetralactam macrocycle with appended targeting ligands is threaded onto a fluorescent squaraine scaffold **S** that is flanked by polyethylene glycol (PEG) chains to give a pre-assembled fluorescent probe (Figure 1). A scaffold with two linked squaraine stations (**S3S**) can accommodate two copies of the macrocycle and thus produce a fluorescent probe with twice the number of targeting units. The threaded structures have high mechanical stability in water and biological media, with no evidence of probe breakdown after 24 hours in a living mouse. The pre-assembled probes absorb light at ~675 nm and emit fluorescence at ~715 nm, which makes them suitable for cuvette experiments using spectroscopic techniques and also for cell microscopy and in vivo imaging studies using the common Cy5 or Cy5.5 filter sets.

Our first biological imaging report using this new class of pre-assembled multivalent probes employed bone-seeking iminodiacetate units as the targeting units.[12] A functionalized macrocycle was threaded onto squaraine scaffolds with one or two docking stations to create

a hexavalent probe with six iminodiacetate ligands and a dodecavalent probe with twelve iminodiacetates. Imaging experiments using living mice found that; (a) the dodecavalent probe produced higher fluorescent staining of the mouse skeleton, and (b) the dodecavalent probe with two squaraine stations was partially self-quenched in aqueous solution and that fluorescence appeared to turn-on when the probe associated with the bone surface. Quantitative studies of these important aspects of multivalent probe targeting were not possible due to the solid and heterogeneous nature of the bone samples. This experimental limitation motivated us to design an alternative probe targeting system that was more amenable for study in homogeneous solution. We decided to build on our accumulated knowledge of the membrane targeting abilities of fluorescent molecular probes with appended zinc(II) dipicolylamine (ZnDPA) coordination complexes.[13–18] We have previously demonstrated that fluorescent ZnDPA probes can selectively target anionic bilayer membranes and distinguish them from the near neutral membranes that are characteristic of healthy mammalian cells. The chelated zinc(II) cations within the ZnDPA units form relatively strong but reversible coordination bonds with the negatively charged phospholipids and phosphorylated amphiphiles that are buried in the anionic membranes. This membrane selectivity is biomedically important since anionic cells are a hallmark of many different types of disease. For example, the surfaces of microbial cells are anionic, as are dead and dying mammalian cells. Thus, fluorescent ZnDPA probes can be used to image various forms of microbial infection and different types of diseased tissue that have high levels of cell death.[17]

The goal of this present study was to compare the membrane and cell targeting properties of the four pre-assembled fluorescent probes in Figure 2. The two targeted probes were hexavalent, **6Z ⊃ S** and dodecavalent **2(6Z) ⊃ S3S** with six and twelve ZnDPA targeting ligands, respectively. The other two fluorescent probes were the non-targeted control molecules, **6C ⊃ S** and **2(6C) ⊃ S3S**, with six and twelve carboxylate groups. A series of cuvette experiments, cell microscopy studies, and in vivo imaging techniques were employed in a complementary fashion to achieve a set of specific aims that included measurement of bilayer membrane binding affinities and characterization of probe multivalent targeting properties. We also conducted biological imaging experiments that assessed probe stability and imaging selectivity in different types of microbial and mammalian cell culture, as well as in a living rat tumor model. The experiments were designed to better understand the performance features of this new class of pre-assembled multivalent probes for selective near-infrared fluorescence imaging of biological targets.

RESULTS AND DISCUSSION

Pre-Assembly of Fluorescent Probes

The chemical syntheses of macrocycle **6C** and squaraine scaffolds **S** and **S3S** were described in our previous study.[12] The new building block, macrocycle **6Z** with six appended ZnDPA units, was prepared in good yield using copper catalyzed cycloaddition chemistry as described in the Supporting Information. Separate stock solutions of the four fluorescent probes shown in Figure 2 were prepared by self-assembly of the respective building blocks. In short, an aqueous solution of **6Z** (250 μM) was mixed at room temperature with an

equimolar solution of squaraine scaffold, **S**, and a spontaneous high-affinity threading process produced the pre-assembled hexavalent probe, **6Z ⊃ S** in a few minutes. Quantitative formation of the threaded structure was confirmed by ^{1}H NMR and MALDI mass spectrometry and also diagnostic changes in squaraine optical properties, including a characteristic 20–30 nm red-shift in absorption and fluorescence maxima, and efficient energy transfer from the excited anthracene side-walls in the surrounding macrocycle to the encapsulated squaraine dye. A stock solution of the dodecavalent probe, **2(6Z) ⊃ S3S** was pre-assembled using an equivalent mixing procedure. That is, two copies of macrocycle **6Z** were threaded onto scaffold **S3S** (250 μM) whose structure contained two squaraine stations connected by a triethyleneglycol linker. Analogous pre-assembly methods were used to produce stock solutions of the control, non-targeted probes **6C ⊃ S** and **2(6C) ⊃ S3S**. The photophysical properties of the four fluorescent probes in water (3 μM) are listed in Table 1 and the associated spectra are provided in the Supporting Information (Figures S1–5). The fluorescence quantum yield of dodecavalent **2(6Z) ⊃ S3S** (Φ_f = 0.02) with two linked squaraine stations, was found to be five times lower than hexavalent **6Z ⊃ S** (Φ_f = 0.10) with a single squaraine. The same trend was observed with the control probes **6C ⊃ S** and **2(6C) ⊃ S3S**. Two supramolecular factors could be contributing to the partial quenching of the dimeric probes with two linked squaraines. One possibility is self-aggregation of the dimeric probes in water, but probe brightness (defined as $\varepsilon \times \Phi_f$) was found to be concentration independent making this an unlikely explanation. Alternatively, the dimeric probes could adopt folded conformations that place the two squaraines in proximal locations that promote non-radiative transfer of the excited state energy (homo-FRET). Strong literature support for this premise are two recent reports that fluorescent molecular probes containing two linked squaraine dyes (not threaded by macrocycle) are strongly quenched in water due to stacking of the two hydrophobic squaraine fluorophores as intramolecular H-aggregates.[19,20] Furthermore, the fluorescence for these dimeric squaraine probes was shown to be enhanced when they unfolded upon interaction with bilayer membranes.

Liposome Association Studies

A series of liposome titration experiments were designed to characterize the interaction of the four different probes in Figure 2 with the surfaces of zwitterionic or anionic liposomes. The liposomes were unilamellar vesicles made by hydration of a thin film of phospholipid, followed by extrusion of the dispersion through an inorganic nanoporous membrane. To ensure experimental consistency, the same phospholipid compositions were used in all experiments; that is, the zwitterionic liposomes were comprised of POPC and the anionic liposomes were a mixture of POPC and POPS (80:20).

The first set of liposome titration experiments tested the related hypotheses that; (a) the pre-assembled probes containing two linked squaraine stations are partially folded and quenched in water, and (b) probe binding to a target surface such as an anionic membrane, leads to probe unfolding and turn-on fluorescence (Figure 3). The fluorescence emission at 710 nm for each of the four pre-assembled probes (250 nM) was measured in the presence and absence of a large excess of zwitterionic or anionic liposomes (1 mM total phospholipid in each case) (Figure 4 and S6). None of the probes have affinity for zwitterionic liposomes and, as expected, the fluorescence of each probe was unchanged by addition of zwitterionic

liposomes. Since the targeted probe **6Z ⊃ S** only has one squaraine dye, it cannot self-quench and the fluorescence intensity was the same in the presence and absence of anionic liposomes (Figure 4 *left*). In the case of **2(6Z) ⊃ S3S**, whose structure contains two threaded squaraine stations, the presence of anionic liposomes produced a 4-fold increase in fluorescence (Figure 4 *right*). As expected, the presence of anionic liposomes had no effect on the fluorescence of control probes **6C ⊃ S** and **2(6C) ⊃ S3S**. These results strongly suggest that the pre-assembled probes containing two linked squaraine stations are partially folded and quenched in water. When the targeted version **2(6Z) ⊃ S3S** associates with anionic liposomes, it partially unfolds on the membrane surface which produces a 4-fold increase in fluorescence (Figure 3), such that **2(6Z) ⊃ S3S** becomes equally as bright on the membrane surface as the targeted probe **6Z ⊃ S**. It is important to note that the experiments in Figure 4 used a large excess of liposomes to guarantee that probe occupancy on the membrane surface was very low. This ensured that intermolecular energy transfer between proximal probe molecules on the membrane surface was unlikely, in contrast to the next liposome system to be discussed.

The second set of liposome titration experiments measured probe affinity to the liposomes using a well-established Fluorescence Resonance Energy Transfer (FRET) titration assay.[16] As shown in Figure 5, probe association with the liposome surface enables efficient FRET from a lipophilic $DiIC_{18}$ donor fluorophore (ex/em: 480/568 nm) embedded in the membrane to a squaraine acceptor fluorophore (ex/em: 675/715 nm) within the probe structure. Each of the four probes were titrated into separate solutions of zwitterionic or anionic liposomes containing the $DiIC_{18}$ donor. Thus, a set of eight titration spectra were generated (Figure S7). The only two titrations that indicated moderate to strong probe affinity were additions of targeted **6Z ⊃ S** or **2(6Z) ⊃ S3S** to anionic liposomes (Figure 6). The loss of $DiIC_{18}$ fluorescence at 568 nm (FRET donor) reflects probe association with the liposome surface, and inspection of the titration isotherms for **6Z ⊃ S** or **2(6Z) ⊃ S3S** (Figure S8) clearly indicates that membrane affinity for the dodecavalent probe is higher than the hexavalent probe. Two possibilities explain this observation – greater affinity due to the higher number of ZnDPA targeting units in the sample or a multivalent probe binding effect.[21] As discussed in the next paragraph, probe association with the membrane surface involves multiple equilibria. Because of the high number of variables, a meaningful fitting of the $DiIC_{18}$ quenching curve is not possible. Therefore, we re-plotted the isotherms as a function of total ZnDPA targeting unit added during the titration (Figure 7), and determined the concentration of added ZnDPA targeting unit required to achieve 50% of saturated binding. The values were ~150 nM and ~500 nM for the dodecavalent **2(6Z) ⊃ S3S** and hexavalent **6Z ⊃ S** probes, respectively. In other words, the binding strength of an individual ZnDPA targeting unit on dodecavalent **2(6Z) ⊃ S3S** is more than three times greater than on hexavalent **6Z ⊃ S**. A major reason for this strong multivalent effect is the high lateral mobility of the anionic POPS within the bilayer. This allows a larger domain of POPS to cluster around the more cationic **2(6Z) ⊃ S3S** which maximizes the average number of coordination bonds with each ZnDPA unit and enhances the secondary electrostatic attraction.[22]

The second major band in the FRET titration spectra in Figure 6 corresponds to the appearance of squaraine fluorescence at 720 nm (FRET acceptor). As expected for the six probe titration systems with weak liposome affinity, there was a gradual increase in probe acceptor fluorescence due to the trivial process of squaraine absorption and re-emission of $DiIC_{18}$ fluorescence. In contrast, the strong binding of probes **6Z ⊃ S** or **2(6Z) ⊃ S3S** to anionic liposomes produced nonlinear isotherms with two distinct transition points (Figure 8). Initially there was fluorescence increase due to probe binding to the liposome surface and accepting energy (FRET) from the embedded $DiIC_{18}$. After a transition point (TP1) in the isotherm the fluorescence decreased due to increasing amounts of intermolecular energy transfer between nearby probe molecules on the liposome surface (homo-FRET). We have observed this surface enhanced probe self-quenching phenomenon before with other multivalent near-infrared fluorescent ZnDPA probes.[16] Probe self-aggregation on the membrane surface is triggered by electrostatic neutralization of the cationic ZnDPA units when they associate with the anionic POPS. The amount of self-aggregated probe on the membrane surface increases until the liposome surface is saturated with probe. Beyond this second transition point (TP2), further probe addition to the sample simply produces the same gradual increase in fluorescence seen with the other six weak association systems. Inspection of the two plots in Figure 8 shows that both transition points occur at lower probe concentrations with dodecavalent **2(6Z) ⊃ S3S** than with hexavalent **6Z ⊃ S**. This is because the dodecavalent probe has a higher membrane affinity and a greater propensity for self-aggregation on the membrane surface. The difference in concentration-dependent probe self-aggregation is due to two structural features; (a) the fluorescent core of the dodecavalent probe is larger and has increased aromatic surface area,[23] (b) the two PEG_{44} chains that flank the hexavalent probe are much longer than the two PEG_3 chains that flank the dodecavalent probe and more effectively hinder self-aggregation.

Taken together, the results of the liposome titration studies indicate that dodecavalent **2(6Z) ⊃ S3S** probe; (a) has higher affinity for anionic membranes than hexavalent **6Z ⊃ S**, due in part to a multivalent binding effect, (b) is folded and partially quenched in water, but this state is reversed upon liposome association, (c) has a greater propensity to self-aggregate on the membrane surface than **6Z ⊃ S**, leading to increased self-quenching due to homo-FRET between adjacent probe molecules. The generalized supramolecular picture that emerges is shown in Figure 9. Association with a target membrane surface favors probe unfolding and a turn-on fluorescence effect that, in principle, could produce high contrast imaging with low signal to background. However, the effect is countered by probe self-aggregation on the surface which promotes quenching and lowers the fluorescence signal intensity.[16]

Microscopic Imaging of Anionic Cells

After demonstrating the selective targeting of **6Z ⊃ S** and **2(6Z) ⊃ S3S** to anionic liposome membranes, the next step was to determine if the pre-assembled probes could be used to image cells with anionic surfaces. The first cells studied were apoptotic mammalian cells whose surfaces become anionic due to exposure of phosphatidylserine during the programmed cell death process.[24] Cell apoptosis was created by treating rat prostate adenocarcinoma (PAIII) cells with non-specific kinase inhibitor staurosporine (500 nM) for 5 hours. Separate samples of staurosporine-treated or untreated cells were incubated with 1

μM of **6Z ⊃ S** or **2(6Z) ⊃ S3S**, and costained with the live-cell indicator CalceinAM (5 μM) and the nuclear indicator Hoechst33342 (3 μM) for 10 minutes, followed by washing and fluorescence microscopy. As expected, the microscopy revealed no staining of healthy PAIII cells by **6Z ⊃ S** or **2(6Z) ⊃ S3S** (Figure S9) but there was selective staining of the dead and dying cells caused by the staurosporine treatment (Figure 10). A comparison of the micrographs showed that the fluorescence intensity of dead cells labeled by **6Z ⊃ S** was higher than cells labeled by **2(6Z) ⊃ S3S**. Visual inspection of the two cell populations indicated that they were both equally stained by the blue-colored probes. Bearing in mind the liposome titration results above, it appears that the lower fluorescence intensity from dead/dying cells labelled with **2(6Z) ⊃ S3S** is due to increased probe self-aggregation and self-quenching on the cell surface. Support for this explanation is the observation that fluorescence intensity from dead/dying cells actually increased when they were labeled with a lower concentration of **2(6Z) ⊃ S3S** (Figure S10). The amount of probe self-quenching on the dead/dying cells is quite high considering that the fraction of exposed phosphatidylserine on the exterior surface of dead/dying cells is typically <10%. However it is important to note that the exposed phosphatidylserine is not distributed evenly across the cell surface but confined to a large degree within small diameter lipid rafts.[25] The high local concentration of phosphatidylserine within these lipid rafts is likely a factor that promotes probe self-aggregation and self-quenching.

We next compared the abilities of **6Z ⊃ S** and **2(6Z) ⊃ S3S** to label the surfaces of microbial cells that are rich in anionic phosphorylated amphiphiles. The pre-assembled fluorescent probes were incubated with separate cultures of two bacterial species, Gram-positive *Streptomyces chromofuscus* (*S. chromofuscus*), and Gram-negative *Escherichia coli* (*E. coli*), and two parasitic protozoa, *Leishmania major* (*L. major*) and *Trypanosoma cruzi* (*T. cruzi*). As shown in Figure 11 and S11, there was no staining of any microbial cell by the control probe **6C ⊃ S**. But in contrast to the results above with dead/dying mammalian cells, there was a consistent trend of moderate staining of all microbial species by **6Z ⊃ S** and very strong staining by **2(6Z) ⊃ S3S**. Two factors likely contribute to this difference. One is due to the weaker affinity that ZnDPA probes have for the anionic amphiphiles in the microbial envelope.[17] At probe dose of 5 μM, there is simply more microbial cell binding by dodecavalent **2(6Z) ⊃ S3S** than hexavalent **6Z ⊃ S**. Furthermore, there is little self-quenching of **2(6Z) ⊃ S3S** after it associates with the microbial surface. In the bacterial envelope, there is a rich and uniform distribution of anionic amphiphiles such as lipoteichoic acid, lipid A, phosphatidylglycerol or cardiolipin,[26,27] and in the protozoan envelope there are high levels of lipophosphoglycan.[28] These abundant anionic microbial amphiphiles disperse the associated probe much more than the localized clusters of phosphatidylserine in the plasma membrane of dead and dying mammalian cells. It is worth noting that our previous imaging study using multivalent bone-seeking probes found no evidence for probe self-quenching on the bone surface.[12] The probe target in the bone was the immobilized Ca(II) distributed throughout the mineral lattice. Self-aggregation of the immobilized probe/Ca(II) complex cannot occur and thus there is no probe self-quenching.

Rat Tumor Imaging Studies

The last goal of the study was to determine if a pre-assembled ZnDPA probe maintains sufficient mechanical stability for effective fluorescence imaging of dead and dying tissue in a living subject. To avoid any ambiguity due to a possible probe concentration effect we excluded the dimeric probe **2(6Z) ⊃ S3S** and focused on pre-assembled probes with only one squaraine. The study employed a syngeneic rat tumor model that it is known to develop a necrotic core that can be targeted by ZnDPA probes.[29] The PAIII cells used in the cell microscopy studies above were injected subcutaneously into the right flank of Lobund Wistar rats and a tumor grew over 14 days. The rats were separated into two cohorts and each rat was intravenously injected with aqueous solutions of targeted **6Z ⊃ S** or untargeted control **6C ⊃ S** (20 nmol). After 24 hours, the rats were euthanized and the excised organs were placed in a whole-body, small animal imaging station that was configured for epifluorescence imaging using the Cy5 filter set. The fluorescence images were used to quantify the biodistribution of near-infrared probe in each organ. The results in Figure 12 show that there was significantly higher accumulation of **6Z ⊃ S** in the tumors compared to control **6C ⊃ S**. Furthermore, there was a large difference in the probe clearance pathways. The majority of untargeted control probe **6C ⊃ S** cleared through the kidney, whereas, the targeted **6Z ⊃ S** exhibited relatively higher accumulation in the liver, lungs, and spleen. Previous work using standard fluorescent ZnDPA probes (i.e., not pre-assembled using Synthavidin technology) injected into the same tumor model has shown that the probes target the dead and dying tissue in the necrotic tumor core.[29] The enhanced tumor targeting seen with the pre-assembled ZnDPA probe after 24 hours in a living rat agrees with our previous work using a pre-assembled bone-seeking probe in mice,[12] and further demonstrates that the threaded probe structure has sufficient mechanical stability for effective in vivo imaging.

CONCLUSIONS

Synthavidin technology is a powerful new method to self-assemble near-infrared fluorescent probes for biological imaging. Previously, we showed that squaraine containing scaffolds (i.e. **S** and **S3S**) could be threaded with a macrocycle containing bone targeting units to produce multivalent bone-seeking fluorescent probes.[12] Here, we thread the same squaraine containing scaffolds with a quite different macrocycle structure to produce two multivalent probes that target the surfaces of anionic membranes. A systematic comparison of the hexavalent **6Z ⊃ S** and the dodecavalent **2(6Z) ⊃ S3S** finds some performance differences that are likely to be generalizable for this class of pre-assembled probes. Liposome titration experiments showed that the binding strength of an individual ZnDPA targeting unit on dodecavalent **2(6Z) ⊃ S3S** is more than three times greater than on hexavalent **6Z ⊃ S**. In addition, the dodecavalent **2(6Z) ⊃ S3S** with two linked squaraine stations is partially quenched in aqueous solution due to a folded conformation. Probe association with a target surface (anionic membrane) leads to relief of the quenching due to probe unfolding and turn-on fluorescence. This is an attractive probe feature for fluorescence imaging because it may lead to a higher signal to background ratio. But a potential imaging weakness with probes comprised of two or more linked squaraine stations (such as dodecavalent **2(6Z) ⊃ S3S**) is a higher propensity to self-aggregate on the target surface leading to probe self-quenching and

loss of probe fluorescence intensity. This effect was observed during fluorescence microscopy experiments that found low fluorescence intensity from dead and dying mammalian cells that were saturated with **2(6Z) ⊃ S3S**. Conversely, the dodecavalent **2(6Z) ⊃ S3S** was found to be a superior targeted probe for illuminating anionic microbial cells. In this case, the stronger probe affinity (due to multivalent binding) produced higher levels of microbial staining with no indication of probe self-aggregation on the microbial surface. We conclude that the value of pre-assembled probes with multiple linked squaraine stations for biological imaging depends on the specific physical attributes of the biomarker target such as the spatial distance between different copies of the biomarker and the propensity of the probe/biomarker complex to self-aggregate.[30,31] Rat tumor imaging experiments showed successful targeting of fluorescent **6Z ⊃ S** to a localized site of necrotic tumor tissue and thus confirmed the high feasibility of pre-assembled probes produced by Synthavidin technology for effective in vivo imaging.

MATERIALS AND METHODS

Materials

Culture media, fetal bovine serum (FBS), and staurosporine were purchased from Sigma Aldrich. POPC (1-palmitoyl-2-oleoyl-*sn*-glycero-3-phosphocholine) and POPS (1-palmitoyl-2-oleoyl-*sn*-glycero-3-phosphoserine) were purchased from Avanti Polar Lipids. $DiIC_{18}$ (1,1′=dioctadecyl-3,3,3′,3′-tetramethylindocarbocyanine perchlorate) was purchased from Invitrogen Inc. *Escherichia coli* DH5α was a gift from Dr. Holly Goodson and *Streptomyces chromofuscus* was a gift from Dr. Richard Taylor at the University of Notre Dame Department of Chemistry and Biochemistry. *Leishmania major* and *Trypanosoma cruzi* were gifts from Dr. Miguel Morales at the University of Notre Dame Department of Biology. The Supporting Information contains the methods used to prepare the four pre-assembled fluorescent probes (**6C ⊃ S**, **2(6C) ⊃ S3S**, **6Z ⊃ S**, **2(6Z) ⊃ S3S**) and the structural and photophysical characterization.

Liposome Preparation

Appropriate ratios of phospholipids were mixed together in $CHCl_3$ and the solvent removed by argon stream for 5 min at room temperature, followed by a high vacuum for 2 h. The remaining film was hydrated and vortexed for 1 min, then subjected to 10 freeze-thaw cycles using liquid N_2 and a 40°C water bath. The liposomes were extruded 23 times through a membrane (polycarbonate, 200 nm pore size, 19 mm diameter, (Whatman Nuclepore Track-Etch Membrane Filtration Products) at room temperature.

Liposome Studies

Turn-on fluorescence studies were performed using either zwitterionic (100% POPC) or anionic (20% POPS: 80% POPC) liposomes. Separate sample of liposomes were mixed with each probe (**6C ⊃ S, 6Z ⊃ S, 2(6C) ⊃ S3S**, or **2(6Z) ⊃ S3S**) to give a final probe concentration of 250 nM and a final phospholipid concentration of 1 mM. The fluorescence spectra were recorded in triplicate. (Parameters: Ex: 645 nm, Em: 670–750 nm, slit width: 3 mm). FRET studies were performed using liposomes that contained the lipophilic donor fluorophore $DiIC_{18}$ and were either zwitterionic (99% POPC, 1% $DiIC_{18}$) or anionic (20%

POPS, 79% POPC, 1% $DiIC_{18}$). Titrations started with liposomes containing a total of 2 μM phospholipid and added aliquots of either **6C ⊃ S, 2(6C) ⊃ S3S**, **6Z ⊃ S** or **2(6Z) ⊃ S3S** (fluorescence acquisition parameters: DiI Ex: 480 nm, Em: 525–750 nm, slit width: 3 mm). Titration spectra for FRET studies are shown in Figures 6 and S7. This same data was used to construct plots of titration isotherms to show relative quenching of $DiIC_{18}$ fluorescence at 568 nm (F/F_0) vs. ZnDPA probe concentration (nM) (Figures 7 and S8).

Microscopic Imaging of Anionic Cells

Mammalian Cell Death Targeting—Prostate adenocarcinoma (PAIII) cells were cultured in DMEM supplemented with 10% FBS and 1% streptomycin/penicillin in a humidified incubator at 37°C with 5% CO_2. Cells were plated in a 8-well chambered coverglass and grown for 24 h. The media on the cells was replaced with either fresh media (untreated) or staurosporine (500 nM, treated) and incubated for 5 h at 37°C. After incubation, the media and staurosporine were removed from each well. One treated and one untreated well was stained with **6Z ⊃ S** (1 μM), **2(6Z) ⊃ S3S** (1 μM), or **2(6Z) ⊃ S3S** (500 nM) in phosphate buffered saline (PBS, 145 mM NaCl, pH7.4). All cells were costained with live-cell indicator CalceinAM (5 μM) and nuclear indicator Hoechst33342 (3 μM) and incubated at 25°C for 10 min in the dark. After incubation, surrounding solutions were removed and the cells were gently washed with PBS. Fluorescent and brightfield micrographs of the cells were acquired using a Nikon TE-2000U epifluorescence microscope equipped with the following filter sets: UV (ex: 340/80, em: 435/85), GFP (ex: 450/90, em: 500/50), and Cy5 (ex: 620/60, em: 700/75).

Microbial Targeting—The parasites *L. major* and *T. cruzi* were gown as axenic promastigotes and maintained at 27 °C in M199 medium supplemented with 10% FBS. Samples were fixed with 1% formalin in 1.5 mL microcentrifuge tubes followed by centrifugation (3000 rpm, 5 min). The fixed parasites were resuspended in 1 mL sterile PBS and treated for 15 min with **6C ⊃ S**, **6Z ⊃ S** and **2(6Z) ⊃ S3S** (5 μM) and two drops of NucBlue® Fixed Cell ReadyProbes® Reagent (Thermo Fisher). The samples were washed twice with fresh buffer to reduce background fluorescence, dispersed into solution and then onto slides coated in L-lysine followed by a drop of Prolong Gold antifade agent and a glass coverslip. The bacteria *E. coli* (grown in LB broth, overnight) and *S. chromofuscus* (grown in ISPI media, 3 d, 26 °C) were harvested and washed twice with sterile HEPES buffer (pH 7.4). The washed cells were resuspended in PBS at an OD_{600} and separate samples were treated with **6C ⊃ S**, **6Z ⊃ S** and **2(6Z) ⊃ S3S** (5 μM). After incubation for 10 min in the dark (20 °C), the cells were washed with sterile HEPES buffer by centrifugation (8,500 g, 1 min) to remove unbound probe and a drop of the dispersed suspension was placed on a glass slide coated in L-lysine followed by a drop of prolong gold and a glass coverslip. All micrographs were acquired using a Nikon Eclipse TE2000-U epifluorescence microscope with a 60× objective and a Photometrics Cascade 512B CCD. Fluorescence images were captured using Cy5 (ex: 620/60, em: 700/75) filter set.

Rat Tumor Imaging

The animal studies were approved by the University of Notre Dame Institutional Animal Care and Use Committee. Six male Lobund-Wistar (LW) rats (3–4 months of age) were

acquired from the LW breeding colony at the University of Notre Dame. A bolus of PAIII Cells (1×10^6) in 300 μL DMEM was subcutaneously injected in the right rear flank of each rat. After 16 days, the rats were given tail vein injections of either **6Z ⊃ S** or **6C ⊃ S** control (each in 300 μL water, 20 nmol/rat, n=3). After another 24 hours, the rats were anesthetized and sacrificed. The liver, spleen, heart, lungs, kidneys, blood, muscle, were removed as well as the tumor. The organs were placed on a transparent imaging tray and imaged using a Bruker In Vitro Imaging System (IVIS) (Ex/Em Filter: Cy5, Exposure: 3s, f-Number: 2, Binning: 2). Images were processed using ImageJ Software and mean pixel intensity (MPI) was determined by creating a region of interest (ROI) around each organ or tumor. The MPI for each organ was normalized to the fluorescence of muscle tissue, with statistical analysis using a Student's *t*-test.

Supplementary Material

Refer to Web version on PubMed Central for supplementary material.

Acknowledgments

This work was supported by grants from the NSF (CHE1401783 to B.D.S.) and the NIH (R01GM059078 to B.D.S. and T32GM075762 to D.R.R. and F.M.R).

References

1. Srinivasarao M, Galliford CV, Low PS. Principles in the design of ligand-targeted cancer therapeutics and imaging agents. Nat Rev Drug Discovery. 2015; 14:203–219. [PubMed: 25698644]
2. Kobayashi H, Longmire MR, Ogawa M, Choyke PL. Rational chemical design of the next generation of molecular imaging probes based on physics and biology: mixing modalities, colors and signals. Chem Soc Rev. 2011; 40:4626–4648. [PubMed: 21607237]
3. Bae YH, Park K. Targeted drug delivery to tumors: myths, reality and possibility. J Control Release. 2011; 153:198–205. [PubMed: 21663778]
4. Wängler C, Maschauer S, Prante O, Schäfer M, Schirrmacher R, Bartenstein P, Eisenhut M, Wängler B. Multimerization of cRGD peptides by click chemistry: synthetic strategies, chemical limitations, and influence on biological properties. ChemBioChem. 2010; 11:2168–2181. [PubMed: 20827791]
5. Appelhans D, Klajnert-Maculewicz B, Janaszewska A, Lazniewska J, Voit B. Dendritic glycopolymers based on dendritic polyamine scaffolds: view on their synthetic approaches, characteristics and potential for biomedical applications. Chem Soc Rev. 2015; 44:3968–3996. [PubMed: 25519948]
6. Martinez A, Ortiz Mellet C, Garcia Fernandez JM. Cyclodextrin-based multivalent glycodisplays: covalent and supramolecular conjugates to assess carbohydrate-protein interactions. Chem Soc Rev. 2013; 42:4746–4773. [PubMed: 23340678]
7. Grunstein D, Maglinao M, Kikkeri R, Collot M, Barylyuk K, Lepenies B, Kamena F, Zenobi R, Seeberger PH. Hexameric supramolecular scaffold orients carbohydrates to sense bacteria. J Am Chem Soc. 2011; 133:13957–13966. [PubMed: 21790192]
8. Ma X, Zhao Y. Biomedical applications of supramolecular systems based on host-guest interactions. Chem Rev. 2015; 115:7794–7839. [PubMed: 25415447]
9. Liu W, Peck EM, Hendzel KD, Smith BD. Sensitive structural control of macrocycle threading by a fluorescent squaraine dye flanked by polymer chains. Org Lett. 2015; 17:5268–5271. [PubMed: 26452041]
10. Peck EM, Liu W, Spence GT, Shaw SK, Davis AP, Destecroix H, Smith BD. Rapid macrocycle threading by a fluorescent dye-polymer conjugate in water with nanomolar affinity. J Am Chem Soc. 2015; 137:8668–8671. [PubMed: 26106948]

11. Smith BD. Smart molecules for imaging, sensing and health (SMITH). Beilstein J Org Chem. 2015; 11:2540–2548. [PubMed: 26734100]
12. Peck EM, Battles PM, Rice DR, Roland FM, Norquest KA, Smith BD. Pre-assembly of near-infrared fluorescent multivalent molecular probes for biological imaging. Bioconjugate Chem. 2016; 27:1400–1410.
13. Smith BA, Harmatys KM, Xiao S, Cole EL, Plaunt AJ, Wolter W, Suckow MA, Smith BD. Enhanced cell death imaging using multivalent zinc(II)-bis(dipicolylamine) fluorescent probes. Mol Pharm. 2013; 10:3296–3303. [PubMed: 23915311]
14. Rice DR, Plaunt AJ, Turkyilmaz S, Smith M, Wang Y, Rusckowski M, Smith BD. Evaluation of [111In]-labeled zinc-dipicolylamine tracers for SPECT imaging of bacterial infection. Mol Imaging Biol. 2015; 17:204–213. [PubMed: 25115869]
15. Lakshmi C, Hanshaw RG, Smith BD. Fluorophore-linked zinc(II)dipicolylamine coordination complexes as sensors for phosphatidylserine-containing membranes. Tetrahedron. 2004; 60:11307–11315.
16. Clear KJ, Harmatys KM, Rice DR, Wolter WR, Suckow MA, Wang Y, Rusckowski M, Smith BD. Phenoxide-bridged zinc(II)-bis(dipicolylamine) probes for molecular imaging of cell death. Bioconjugate Chem. 2016; 27:363–375.
17. Rice DR, Clear KJ, Smith BD. Imaging and therapeutic applications of zinc(II)-dipicolylamine molecular probes for anionic biomembranes. Chem Commun. 2016; 52:8787–8801.
18. Plaunt AJ, Harmatys KM, Wolter WR, Suckow MA, Smith BD. Library synthesis, screening, and discovery of modified zinc(II)-bis(dipicolylamine) probe for enhanced molecular imaging of cell death. Bioconjugate Chem. 2014; 25:724–737.
19. Karpenko IA, Collot M, Richert L, Valencia C, Villa P, Mély Y, Hibert M, Bonnet D, Klymchenko AS. Fluorogenic squaraine dimers with polarity-sensitive folding as bright far-red probes for background-free bioimaging. J Am Chem Soc. 2015; 137:405–412. [PubMed: 25506627]
20. Yao D, Lin Z, Wu J. Near-infrared fluorogenic probes with polarity-sensitive emission for in vivo imaging of an ovarian cancer biomarker. ACS Appl Mater Interfaces. 2016; 8:5847–5856. [PubMed: 26910257]
21. Kitov PI, Bundle DR. On the nature of the multivalency effect: a thermodynamic model. J Am Chem Soc. 2003; 125:16271–16284. [PubMed: 14692768]
22. Menke M, Gerke V, Steinem C. Phosphatidylserine membrane domain clustering induced by annexin A2/S100A10 heterotetramer. Biochemistry. 2005; 44:15296–15303. [PubMed: 16285733]
23. Zayed JM, Nouvel N, Rauwald U, Scherman OA. Chemical complexity–supramolecular self-assembly of synthetic and biological building blocks in water. Chem Soc Rev. 2010; 39:2806–2816. [PubMed: 20589265]
24. Smith BA, Smith BD. Biomarkers and molecular probes for cell death imaging and targeted therapeutics. Bioconjugate Chem. 2012; 23:1989–2006.
25. Simons K, Sampaio JL. Membrane organization and lipid rafts. Perspect Biol. 2011; 3:a004697.
26. Leevy WM, Johnson JR, Lakshmi C, Morris J, Marquez M, Smith BD. Selective recognition of bacterial membranes by zinc(II)-coordination complexes. Chem Commun. 2006; 15:1595–1597.
27. White AG, Fu N, Leevy WM, Lee JJ, Blasco MA, Smith BD. Optical imaging of bacterial infection in living mice using deep-red fluorescent squaraine rotaxane probes. Bioconjugate Chem. 2010; 21:1297–1304.
28. Rice DR, Vacchina P, Norris-Mullins B, Morales MA, Smith BD. Zinc(II)-dipicolylamine coordination complexes as targeting and chemotherapeutic agents for *Leishmania major*. Antimicrob Agents Chemother. 2016; 60:2932–2940. [PubMed: 26926632]
29. Smith BA, Akers WJ, Leevy WM, Lampkins AJ, Xiao S, Wolter W, Suckow MA, Achilefu S, Smith BD. Optical imaging of mammary and prostate tumors in living animals using a synthetic near infrared zinc(II)-dipicolylamine probe for anionic cell surfaces. J Am Chem Soc. 2010; 132:67–69. [PubMed: 20014845]
30. Kiessling LL, Gestwicki JE, Strong LE. Synthetic multivalent ligands in the exploration of cell-surface interactions. Curr Opin Chem Biol. 2000; 4:696–703. [PubMed: 11102876]

31. Fischer G, Lindner S, Litau S, Schirrmacher R, Wangler B, Wangler C. Next step toward optimization of GRP receptor avidities: determination of the minimal distance between BBN(7–14) units in peptide homodimers. Bioconjugate Chem. 2015; 26:1479–1483.

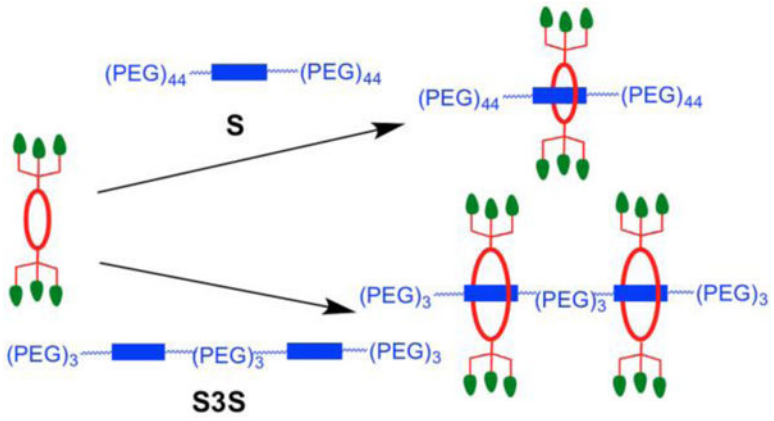

Figure 1.

Pre-assembly of fluorescent probes is achieved by threading a macrocycle (red) with appended targeting units (green) onto a linear scaffold (blue) with a single fluorescent squaraine station **S** or double squaraine station **S3S**.

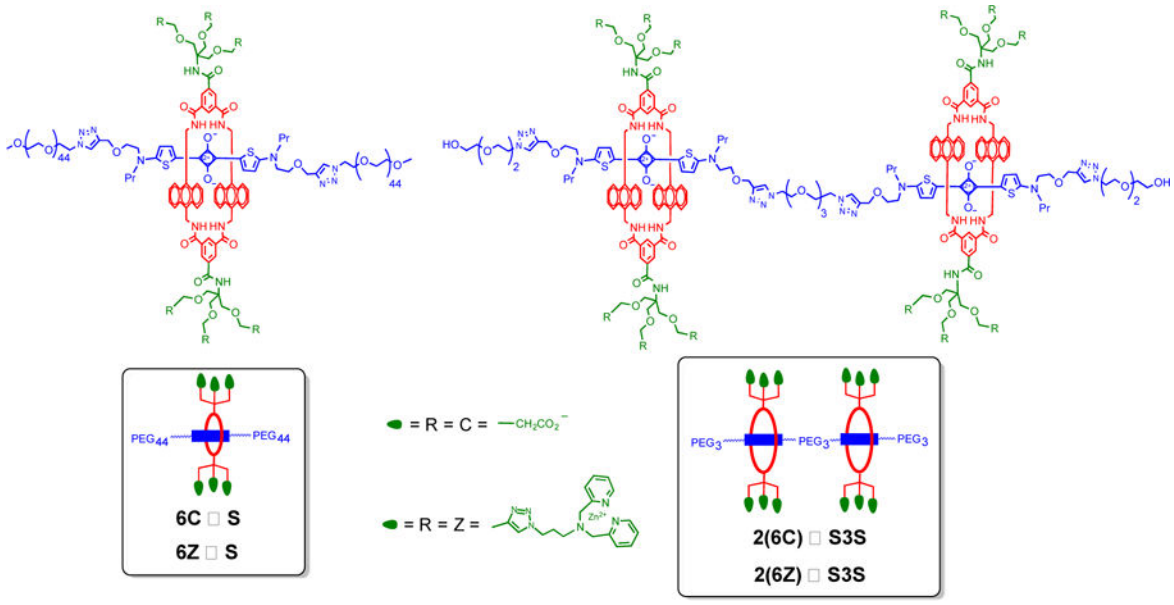

Figure 2.

Structures of the four pre-assembled fluorescent probes used in this study; non-targeted **6C ⊃ S** and **2(6C) ⊃ S3S**, and targeted **6Z ⊃ S** and **2(6Z) ⊃ S3S**.

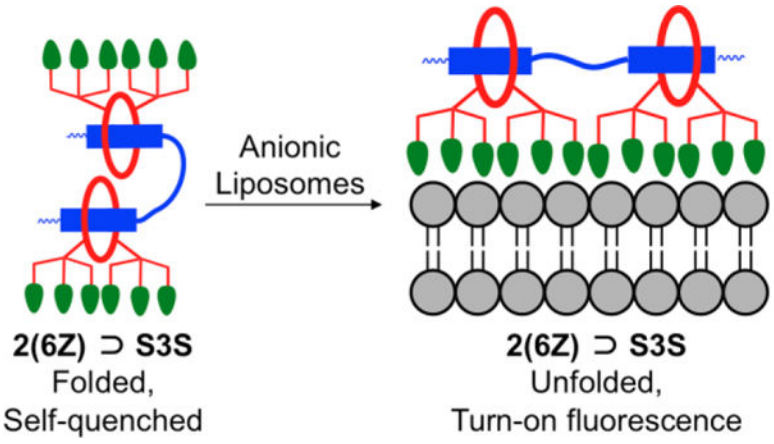

Figure 3.

Representation of **2(6Z) ⊃ S3S** adopting a folded and self-quenched conformation in aqueous solution. Upon association with anionic liposomes the probe unfolds with turn-on fluorescence.

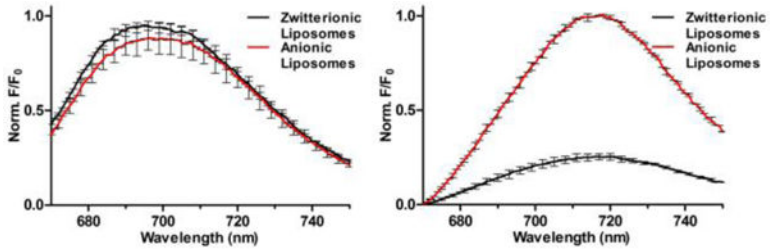

Figure 4.

Fluorescence spectra for **6Z ⊃ S** (*left*) and **2**(**6Z**) **⊃ S3S** (*right*) (250 nM) in the presence of either zwitterionic (100% POPC) or anionic (20% POPS, 80% POPC) liposomes, total phospholipid 1 mM, Ex: 645 nm.

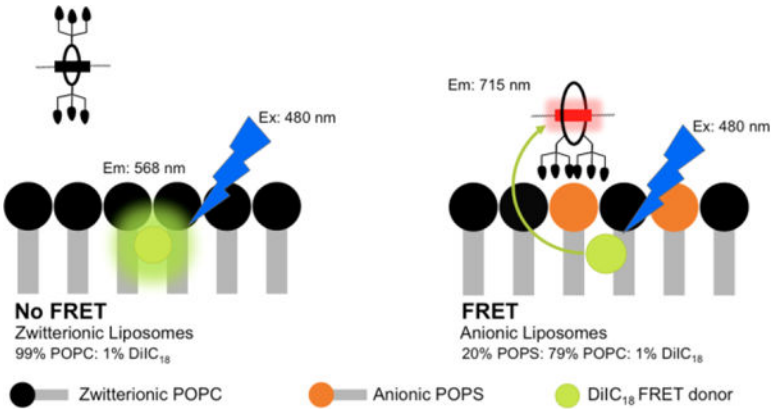

Figure 5.

Illustration of FRET induced by membrane association of fluorescent probe **6Z ⊃ S** (shown) or **2(6Z) ⊃ S3S** (not shown) to anionic liposomes containing 1% $DiIC_{18}$ (Ex/Em 480/568 nm) as the fluorescence energy acceptor. There is no probe association with zwitterionic (100% POPC) liposomes.

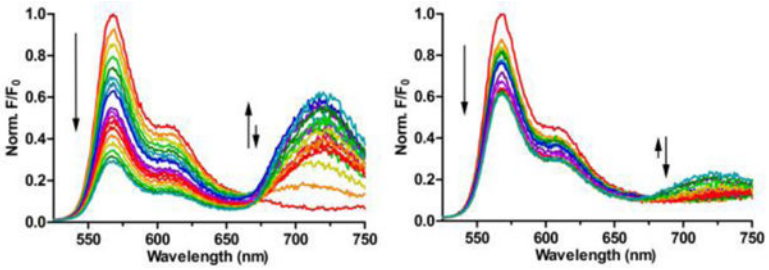

Figure 6.

FRET titration spectra for **6Z ⊃ S** (*left*) and **2(6Z) ⊃ S3S** (*right*) in the presence of anionic liposomes (20% POPS, 79% POPC, 1% $DiIC_{18}$; total lipid concentration 2 μM). Probe concentrations during the titration ranged from 0–800 nM, Ex: 480 nm

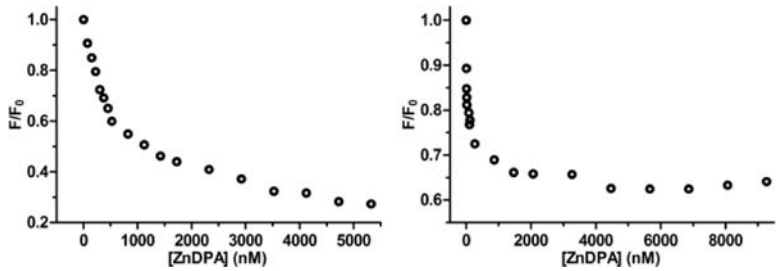

Figure 7.

Titration isotherms for relative quenching of $DiIC_{18}$ fluorescence at 568 nm (F/F_0) due to FRET caused by association of **6Z ⊃ S** (*left*) or **2(6Z) ⊃ S3S** (*right*) with the anionic liposomes (Ex: 645 nm). The unit for the x-axis is total concentration of ZnDPA targeting unit in the sample.

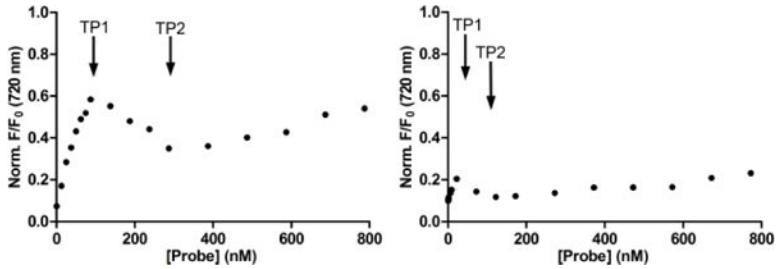

Figure 8.

Change in fluorescence at 720 nm for probes **6Z ⊃ S** (*left*) and **2(6Z) ⊃ S3S** (*right*) during addition to anionic liposomes (20% POPS, 79% POPC, 1% $DiIC_{18}$). TP1 and TP2 are transition points 1 and 2, respectively.

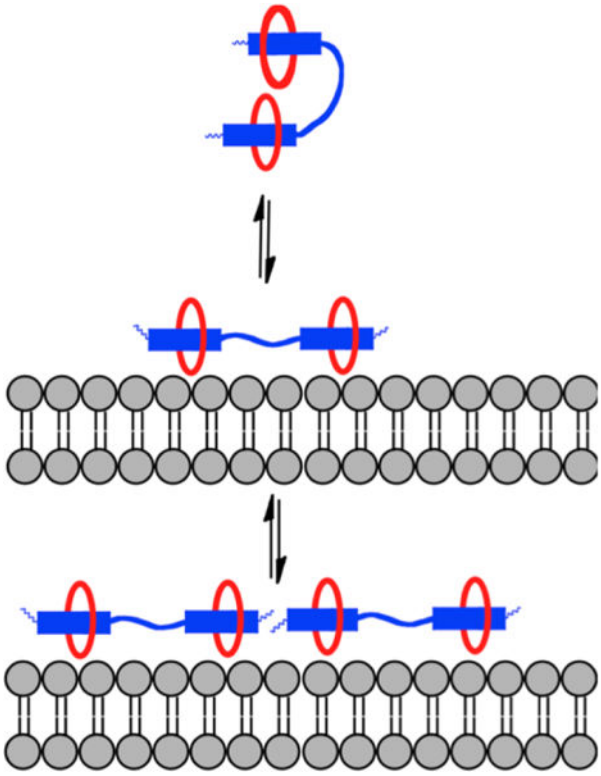

Figure 9.

Generalized picture showing that a pre-assembled probe with two linked squaraines is folded and self-quenched in aqueous solution. Upon association with a target membrane surface, the probe unfolds with turn-on fluorescence but additional probe association with the surface leads to probe self-aggregation and quenching.

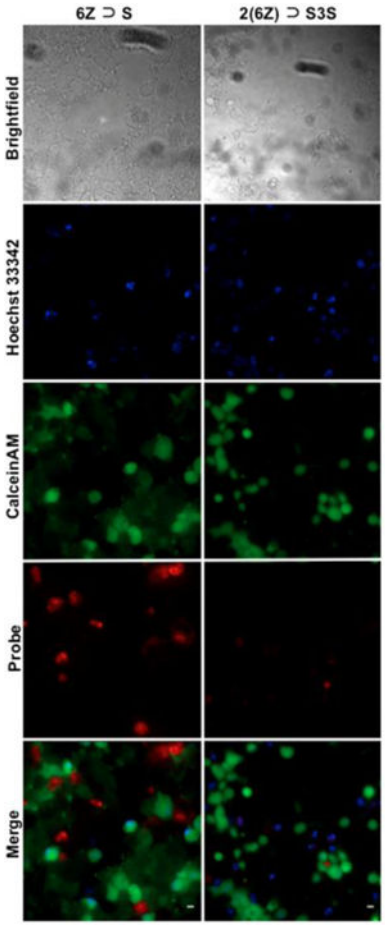

Figure 10.

Fluorescence microscopy images of dead and dying PAIII cells that were caused by cell pre-treatment with staurosporine (500 nM). All cells were stained with deep-red**6Z ⊃ S** (*left*), or **2(6Z) ⊃ S3S** (*right*) (1 μM) and costained with blue nuclear indicator Hoechst33342 (3 μM) and green live-cell indicator CalceinAM (5 μM). Scale Bar = 10 μM.

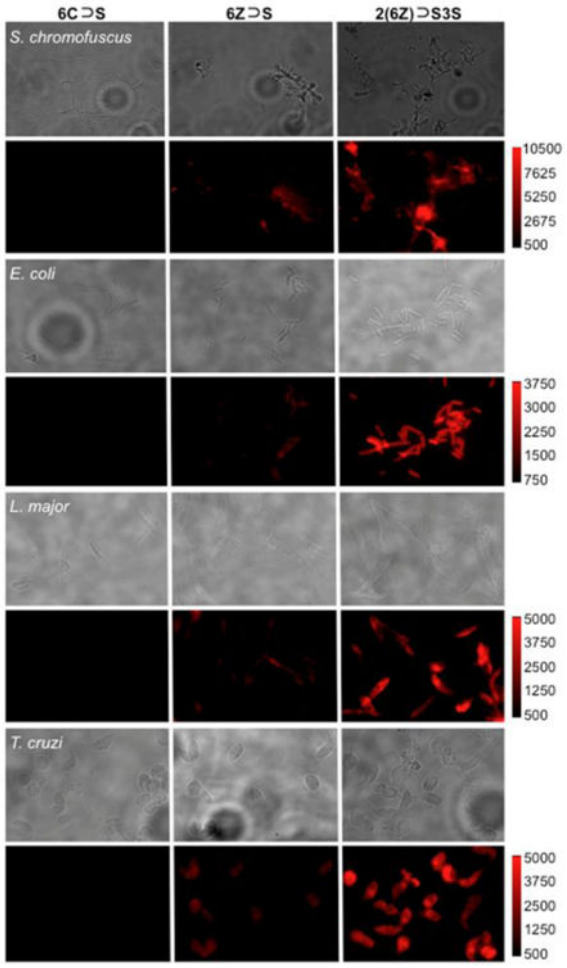

Figure 11.

Fluorescence micrographs of *S. chromofuscus*, *E. coli*, *L. major*, and *T. cruzi*, stained with **6C ⊃ S**, **6Z ⊃ S**, or **2(6Z) ⊃ S3S** (5.0 μM). Brightfield (upper panel) and deep-red probe fluorescence (lower panel). The fluorescence intensity of each image in a row is scaled to the image with **2(6Z) ⊃ S3S**.

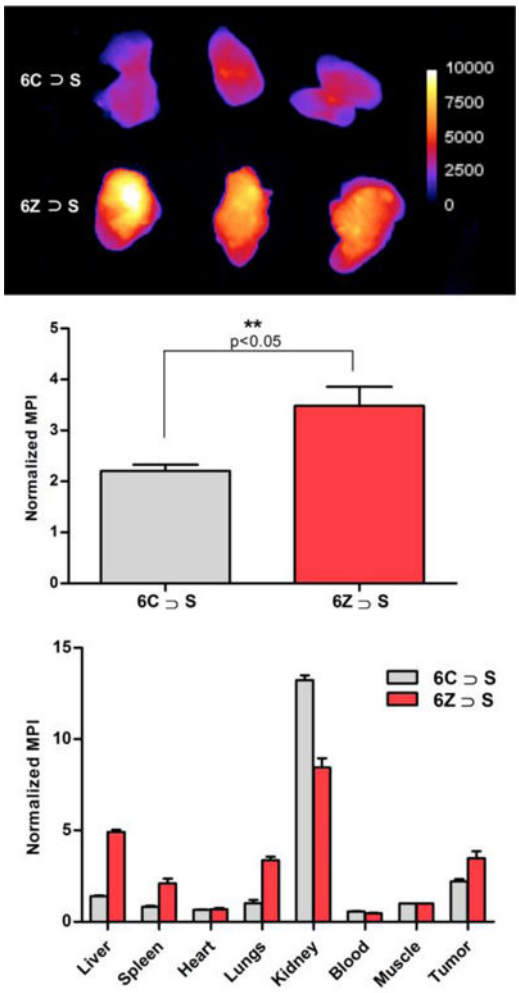

Figure 12.

Biodistribution of **6C ⊃ S** or **6Z ⊃ S** in tumor-bearing rats at 24 hours after probe dosing (20 nmol). (*top*) Fluorescence images of excised tumors (IVIS Cy5 filter set, Exposure 3s, f-Number 2, Binning 2). (*middle*) Quantification of tumor fluorescence as mean pixel intensity (MPI) (n=3, p<0.05). (*top*) Probe biodistribution measured as MPI for each excised organ.

Table 1

Probe photophysical properties in water (3 μM).

probe	λ_{abs} (nm)	λ_{em} (nm)	log ε	Φ_f[a]
6Z ⊃ S	677	715	5.20	0.10
6C ⊃ S	677	710	5.02	0.18
2(6Z) ⊃ S3S	672	719	5.32	0.02
2(6C) ⊃ S3S	673	716	5.36	0.02

[a] relative to methylene blue in water (Φ_f = 0.02).